Parainfluenza Fusion Peptide Promotes Membrane Fusion by Assembling into Oligomeric Porelike Structures

Mariana Valério,[§] Diogo A. Mendonça,[§] João Morais, Carolina C. Buga, Carlos H. Cruz, Miguel A.R.B. Castanho, Manuel N. Melo, Cláudio M. Soares,* Ana Salomé Veiga,* and Diana Lousa*

Read Online

ACCESS | Metrics & More | Article Recommendations | Supporting Information

ABSTRACT: Paramyxoviruses are enveloped viruses harboring a negative-sense RNA genome that must enter the host's cells to replicate. In the case of the parainfluenza virus, the cell entry process starts with the recognition and attachment to target receptors, followed by proteolytic cleavage of the fusion glycoprotein (F) protein, exposing the fusion peptide (FP) region. The FP is responsible for binding to the target membrane, and it is believed to play a crucial role in the fusion process, but the mechanism by which the parainfluenza FP (PIFP) promotes membrane fusion is still unclear. To elucidate this matter, we performed biophysical experimentation of the PIFP in membranes, together with coarse grain (CG) and atomistic (AA) molecular dynamics (MD) simulations. The simulation results led to the pinpointing of the most important PIFP amino acid residues for membrane fusion and show that, at high concentrations, the peptide induces the formation of a water-permeable porelike structure. This structure promotes lipid head intrusion and lipid tail protrusion, which facilitates membrane fusion. Biophysical experimental results validate these findings, showing that, depending on the peptide/ lipid ratio, the PIFP can promote fusion and/or membrane leakage. Our work furthers the understanding of the PIFP-induced membrane fusion process, which might help foster development in the field of viral entry inhibition.
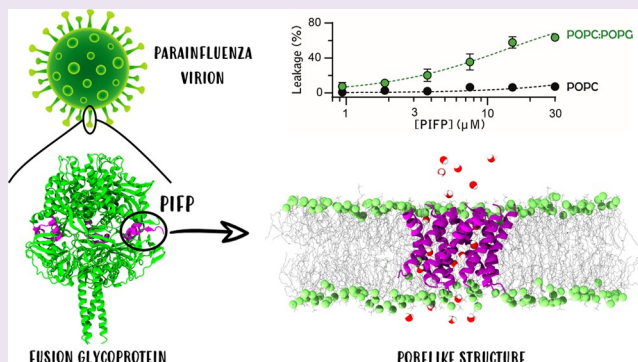
Parainfluenza viruses (PIVs) contribute significantly to the annual global disease burden in humans.[1,2] It is estimated that annually, in the USA alone, parainfluenza infections are responsible for more than 325,000 hospitalizations of children under 5 years old.[3] Although it is difficult to estimate the exact number of infections caused by the PIVs worldwide, these viruses have the potential to infect millions of individuals, leading to an undetermined number of deaths, especially in areas with inadequate health-care resources. To make matters worse, there are no specific treatments for infections caused by PIVs.[1,2]

PIVs belong to the Paramyxoviridae family, consisting of enveloped viruses harboring a negative-sense RNA genome that, like all enveloped viruses, depend on the fusion of the viral envelope with the host cell membrane to infect the host. In the PIVs, the machinery responsible for viral fusion is composed of the receptor-binding glycoprotein hemagglutinin-neuraminidase (HN) and the fusion glycoprotein (F), that, together, form the viral fusion complex.[4]

Opposite to what occurs in the cell entry of the influenza virus,[5] PIVs are not endocytosed by the target cells and instead fuses its membrane with the host membrane at the cell surface (and neutral pH).[6] The membrane fusion process starts with the recognition and binding of the receptor-binding glyco-protein to receptors at the host cell surface. This binding triggers the F glycoprotein to undergo major conformational rearrangements and the proteolytic cleavage of the F protein, exposing the fusion peptide (FP) region (Figure 1A; the PIFPs are highlighted in pink), promoting viral entry.[6,7] After being exposed, this region is inserted into the target membrane[8] and the F protein refolds to form a six-helix bundle (6HB), placing the fusion peptides and the transmembrane domains in proximity, facilitating membrane fusion.[9,10]

Regions with functional requirements for membrane fusion and viral entry, such as the PIFP, are, in general, highly conserved among viral families and contain several hydro-phobic residues (Figure 1B,C, respectively). Another common feature among these sequences is their location within the fusion protein. In class I fusion proteins, they are usually located at their N-terminal end or close to it.[11] All of these traits are also found in the PIFP, together with the presence of GXXXG motifs (Figure 1D). The GXXXG motifs are the
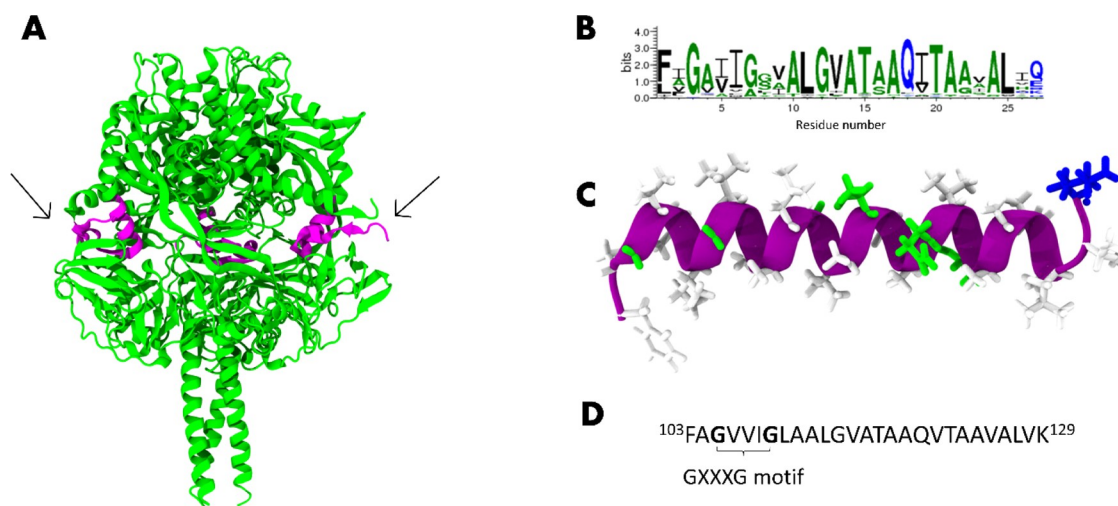
Figure 1. Parainfluenza fusion peptide features. (A) Cartoon representation of the crystal structure of the cleaved prefusion F protein trimer, 4GIP, viewed from the side, with the FP highlighted colored in pink. Arrows indicate the protease cleavage sites. (B) Sequence conservation of glycoprotein F among members of the Paramyxoviridae family. Color is used to show hydrophobicity of the residues (blue: hydrophilic, green: neutral, and black: hydrophobic). (C) Molecular image of the PIFP with the backbone in purple and the residues colored according to their biophysical properties: nonpolar (white), basic (blue), and polar residues (green). (D) PIFP amino acid sequence with the GXXXG motif highlighted.

hallmark of many high-affinity associations between transmembrane helices.[12,13] The presence of these motifs in the PIFP alludes to the possibility that inter-PIFP peptide interactions are common, a hypothesis that was investigated in this work. Interestingly, mutations to these glycine residues in the FP from the paramyxovirus simian parainfluenza virus 5 (SV5) resulted in mutant F proteins with hyperactive fusion phenotypes but not in the human parainfluenza virus 3 (HPIV3).[14]

Most studies regarding the mechanisms of the viral FPs and their interaction with model membranes have focused on influenza virus and human immunodeficiency virus (HIV). Hypotheses for the mechanism by which the FP from these viruses induces membrane fusion suggest different modes of action, including altering the membrane curvature,[15−18] increasing[19−21] or decreasing lipid order,[22,23] and inducing pore formation and/or its stabilization.[18,24,25] Additionally, a mechanism proposed on the basis of molecular dynamics (MD) simulations has shown that lipid tail protrusion (i.e., a lipid acyl chain that extends to and beyond the corresponding phosphate group) is a determinant step in membrane fusion.[24,26] The occurrence of lipid tail protrusion has been observed in several simulation studies of the influenza FP in membrane bilayers, which indicates that the peptide increases the probability of lipid protrusion events.[22,23,27,28] For the influenza virus, it has also been shown that the peptide interacts with the lipid headgroups, mainly through the N-terminal group, which induces these headgroups to penetrate deeper into the membrane (headgroup intrusion).[22,26−28]

Recent experimental data has elucidated the orientation adopted by the PIFP in a membrane bilayer, a determinant for the peptide-induced perturbation of lipid bilayers.[29] NMR structural analysis in 1-palmitoyl-2-oleoyl-glycero-3-phosphocholine (POPC)/1-palmitoyl-2-oleoyl-sn-glycero-3-phosphoglycerol (POPG), 1,2-dioleoyl-sn-glycero-3-phosphocholine (DOPC)/1,2-dioleoyl-sn-glycero-3-phosphoglycerol (DOPG), and 1,2-dioleoyl-sn-glycero-3-phosphoethanolamine (DOPE) membranes showed that the peptide is fully α-helical when inside a POPC/POPG membrane, adopting a mixed strand/

helix conformation in the DOPC/DOPG membrane, and is primarily a β-strand in the DOPE membranes.[30] Regarding the peptide insertion in the membrane, ^{1}H spin diffusion experiments in liquid crystal and gel phases showed that in a POPC/POPG membrane the N-terminal half of the peptide is more exposed to the membrane surface, whereas in a DOPC/DOPG membrane, the C-terminal residues are more exposed to water than the N-terminal residues.[30]

A crucial question remains unanswered: What is the mechanism by which the PIFP promotes membrane fusion? Data on the interaction between PIFPs in phospholipid micelles has shed some light on this matter. When inside a membrane, there seems to be a cooperative and specific assembly of the PIFP into hexamers.[31] Short molecular dynamics (MD) simulations of the hexameric structure also showed that there is penetration of water into its core from the viral side of the membrane.[31]

In this work, we conducted a comprehensive analysis of the effect of peptide concentration on the PIFP properties by combining experimental biophysical data with results from coarse grain (CG) and all-atom (AA) MD simulations. Förster resonance energy transfer (FRET)-based assays revealed that the percentage of peptide-induced lipid mixing and leakage is higher at high peptide/lipid ratio conditions. Circular dichroism (CD) results showed that there is also an effect of concentration on the PIFP secondary structure. The simulation studies elucidated the peptide−peptide interactions that stabilize PIFP inside a mixed bilayer to allow the formation of a porelike structure. Finally, we characterized the peptide−membrane interactions and pinpointed the amino acid residues that are crucial for the peptide's ability to interact with and perturb the host membrane.

This work provides a valuable contribution to understanding the membrane fusion process induced by the PIFP, which can be very useful in the future development of antiviral therapies targeting this virus.
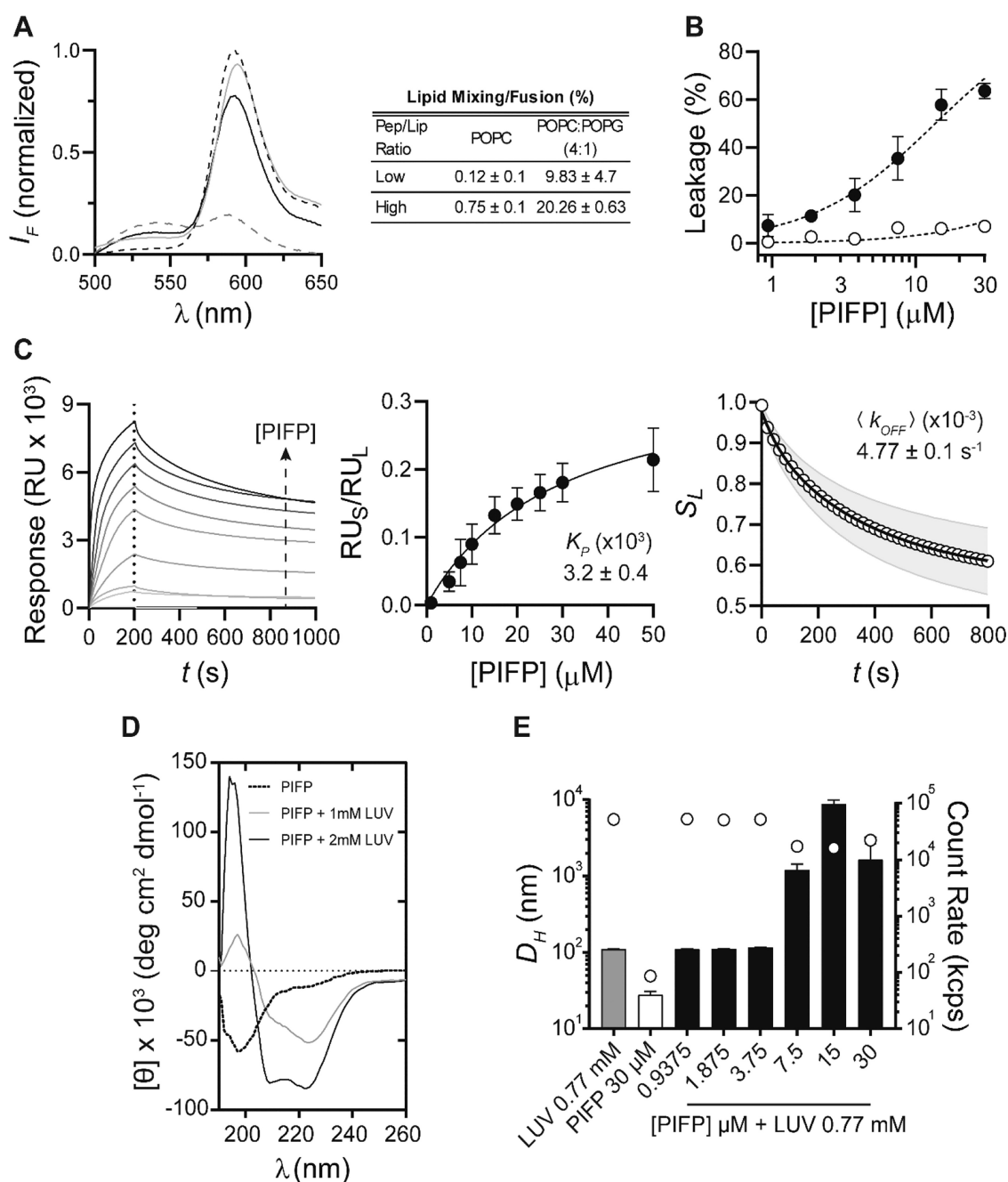
Figure 2. Characterization of PIFP−lipid membrane interactions *in vitro*. (A) Representative FRET PIFP−lipid mixing induction spectra (left) in POPC:POPG (4:1) vesicles (black dashed line, control; gray dashed line, Triton 1% (v/v); gray line, PIFP low pep/lip ratio; black line, PIFP high pep/lip ratio). PIFP−lipid fusion induction (%) (right) was extrapolated from equation 2. (B) PIFP−membrane perturbation induction. Leakage (%) from 0.77 mM large unilamellar vesicles (LUVs) [white, POPC; black, POPC:POPG (4:1)] loaded with 50 mM 5,6-CF was obtained upon incubation with PIFP in concentrations ranging between 0.9375 and 30 μM. (C) Surface plasmon resonance (SPR) PIFP−lipid (un)binding kinetics. (Left) SPR sensorgrams of increasing PIFP concentrations (gray scale, from lighter to darker, 1, 5, 7.5, 10, 15, 20, 25, 30, and 50 μM of PIFP) interacting with POPC:POPG (4:1) small unilamellar vesicle (SUV). A vertical dashed line at 200 s separates association and dissociation phases. (Middle) PIFP partition extends toward POPC:POPG (4:1) SUV. Individual values of RU_S and RU_L were obtained from each PIFP sensorgram at 200 s at the different concentrations tested. Data was fitted with equation 4, from which the K_P value was obtained. (Right) PIFP dissociation kinetics. Membrane-associated PIFP (S_L) was plotted as a function of the dissociation time. Standard deviation interval is represented in gray. The data obtained was fitted by equation 5. (D) PIFP secondary structure. PIFP CD spectra were obtained in aqueous solution and in the presence of 1 and 2 mM of POPC:POPG (4:1) LUV. (E) PIFP and PIFP−LUV aggregation profiles. Z-average D_H (columns) and count rate (circles) of the particles formed upon titration of PIFP in a 0.77 mM POPC:POPG (4:1) LUV solution were obtained by dynamic light scattering (DLS). Particles formed in the presence of 0.77 mM LUV and PIFP 30 μM sample solution were obtained as controls.
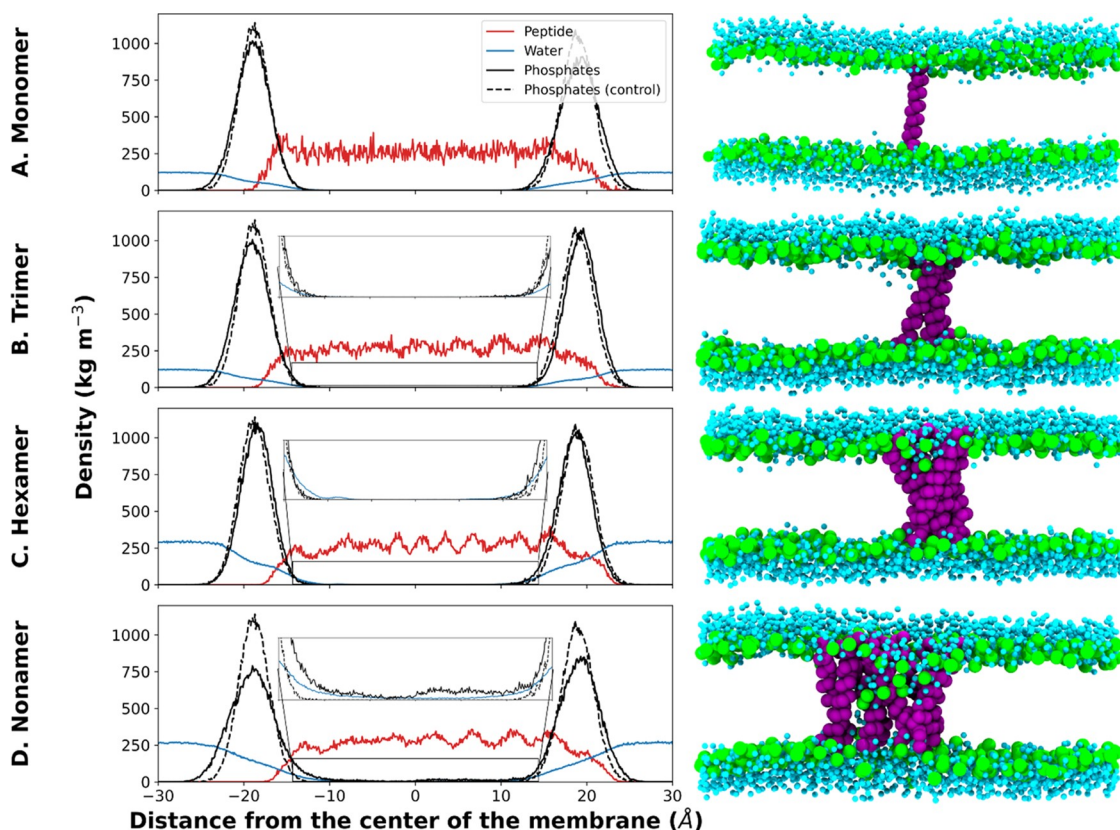
Figure 3. Density profiles obtained from CG simulations of the PIFP. The density profiles for the four systems with increasing peptide/lipid ratios (monomer < trimer < hexamer < nonamer) show the overall behavior of the system components during the simulation. The dashed lines represent the phosphate densities in systems without peptides; the solid lines are all relative to the systems with the PIFPs. The images on the right side are snapshots of the last frame of CG simulations, where the PIFPs are shown in purple, water molecules in blue, and the lipid phosphate groups in green.

RESULTS

PIFP Induces Fusion and Perturbation on Negatively Charged Lipid Vesicles. PIFP conformational properties and effects on lipid membranes are still unclear. To fill this gap, we synthesized the PIFP that corresponds to residues 103−129 of the PIV5 F protein bound to an 8-amino-3,6-dioxaoctanoic acid conjugated to a polylysine tail (FAGVVIGLAALGVA-TAAQVTAAVALVK-AEEAc−KKKK) and characterized its structure and interaction with lipid membranes using an array of biophysical methodologies.

Given its potential fusogenic properties, we first evaluated the PIFP ability to induce fusion and perturbation on lipid vesicles. In this study, we wish to understand the role played by lipid charge in the PIFP ability to induce membrane fusion, and for that reason, we compared POPC vesicles with POPC:POPG (4:1) vesicles. Fusion was followed by PIFP-induced FRET efficiency variations in a mixture containing NBD-RhB-doped vesicles (donor and acceptor, respectively) and nondoped vesicles,[32] while the membrane perturbation was followed by the PIFP-induced leakage of 5,6-carboxy-fluorescein (5,6-CF)-loaded vesicles. Despite the inability to induce fusion or leakage from zwitterionic POPC vesicles, PIFP induces fusion and leakage on anionic POPC:POPG (4:1) vesicles (Figure 2A,B). Besides its hydrophobic nature, PIFP is also cationic, with a net charge of +5 at pH 7.4, which contributes to the membrane charge-action dependence observed, not unique within fusion peptides.[33] Moreover, PIFP induces 9.83% of lipid fusion at the low peptide/lipid

ratio condition (membrane nonsaturated condition) and 20.3% of lipid fusion at the high peptide/lipid ratio condition (membrane saturation condition), an approximately 2-fold increase, suggesting that the fusion efficiency is also influenced by the local concentration of the peptide on the membrane. The same pattern is observed for the membrane perturbation phenomena, on which 5,6-CF leakage increases in a PIFP-concentration-dependent fashion. These results may indicate the presence of peptide−peptide interactions, such as self-association/clustering or conformational changes, which eventually lead to a pore formation, that may play a major role in the fusion process of PIFP. To answer this question, PIFP−lipid interactions were thoroughly characterized *in vitro*.

PIFP−Lipid Unbinding Follows a Second-Order Kinetics. After demonstrating that PIFP is fusogenic, it was of utmost importance to unravel its fusion mechanisms. As the fusion process is guided by the interactions between the peptide and the lipid molecules present in the membrane,[34] we first characterized the lipid binding of PIFP. Anionic POPC:POPG (4:1) vesicles were used for peptide−membrane interaction characterization assays since PIFP is only capable of inducing the fusion of vesicles with this composition.

Peptide−lipid binding was evaluated through surface plasmon resonance (SPR). This technique allows real-time detection of bound molecules on a small unilamellar vesicle (SUV)-covered surface coupled with a flow system. Peptide-to-lipid response ratios were plotted as a function of the injected peptide concentration, allowing an estimation of the peptide

partition coefficient (K_P), as described elsewhere.[35] PIFP exhibits high lipid binding responses, in a concentration-dependent fashion (Figure 2C, left panel), leading to a $K_P \approx 3.2 \times 10^3$ (Figure 2C, middle panel). Given the PIFP fusion capacity, a K_P of this magnitude—similar to values described for other fusion peptides[36]—was expected.

The sensorgram analysis also shows that there are variations in the dissociation kinetics (200−1000 s after injection) with the increasing peptide concentration, especially comparing the 30 and 50 μM PIFP sensorgrams. For this reason, PIFP−membrane dissociation kinetics were further evaluated. PIFP−membrane dissociation follows a second-order kinetics, most likely derived from the presence of two peptide populations (Figure 2C, right panel): one faster, with lower mass and decreased retention, most likely corresponding to the individual peptide molecules; and another slower, with higher mass and increased retention, most likely corresponding to clusters formed by peptide molecules. Accompanied by a significant variability within the concentration range, the dissociation kinetics analysis suggests the presence of peptide−peptide and/or peptide−lipid aggregation dependent on the PIFP concentration. The weight-averaged dissociation constant ($<k_{off}>$) extrapolated is $\approx 4.77 \times 10^{-3}$ s^{-1}, which is in fact quite similar to the $<k_{off}>$ described for an aggregation-prompt peptide observed by Figueira et al.[35] The PIFP−lipid binding analysis reinforces the argument of an oligomerization/aggregation process present on the PIFP fusion mechanism. However, the macromolecular organization of the peptide−vesicle aggregates was still inconclusive.

PIFP Helix Content Depends on the Membrane Saturation Level. Another relevant aspect to evaluate is the PIFP secondary structure, not only in solution but also upon interaction with lipids.[34] Similar to other fusion peptides, PIFP evolves from a mainly random-coil conformation in aqueous solution to a α-helical conformation upon interaction with anionic POPC:POPG (4:1) membranes (Figure 2D).

Additionally, we also observe that the PIFP α-helix content in the presence of large unilamellar vesicles (LUVs) depends on the lipid concentration. This can be inferred from (i) the existence of more than one isosbestic point in the spectra of Figure 3 and (ii) from the obvious departure from an α-helical spectrum in the 205−225 nm range at 1 mM of LUVs, where the spectrum minima are distorted. Note that, at 1 mM, a mixture of aqueous- and membrane-bound peptide populations is expected (for a $K_P \approx 3.2 \times 10^3$ and 1 mM lipid, about 30% of the peptide is expected to be unbound[37]); still, the spectrum at 1 mM lipid in Figure 2D cannot be explained by a combination of those at 0 and 2 mM lipids (hence the multiple isosbestic points), indicating the existence of at least a third population with different structural characteristics. Importantly, it is at lower lipid concentrations that the PIFP reaches the highest local peptide/lipid ratios in the membrane, which seem to be the conditions for this third, less helical population to occur. The relevance of these different peptide populations is discussed below.

Vesicle Aggregation Triggering Is Dependent on the PIFP Concentration. Membrane-surface peptide aggregation/oligomerization is commonly shared between viral fusion peptides.[38] The increased local peptide concentration on the membrane's surface enhances the destabilization of lipid−lipid interactions and associated membrane tension, promoting the mixture of the viral and host cell membrane lipid content or, in other cases, the formation of a pore.[39] However, the fusion

peptide aggregation/oligomerization process differs between viruses, with direct impact on its fusion mechanism. PIFP revealed the tendency to accumulate on the lipid vesicle surface in a concentration-dependent fashion, perturbating its membranes and promoting the fusion between anionic vesicles. However, the aggregation profile of both PIFP alone and PIFP−LUV structures was still unclear. Using dynamic light scattering (DLS), we characterized the macromolecular organization of these structures. Hydrodynamic diameter (D_H) and particle count rate were obtained upon PIFP consecutive addition to a 0.77 mM lipid vesicle solution (Figure 2E).

Three important observations are worth mentioning: (1) PIFP does not form aggregates in aqueous solution; (2) upon increasing the PIFP concentration from 3.75 to 7.5 μM, the LUV particles grow, at least, 10-fold on its D_H, with a high variability on their sizes (Figure S1); and (3) in parallel with this particle size increase, the particle count suffers an approximately 5-fold reduction. These results suggest that upon reaching a critical aggregation concentration (CAC), between 3.75 and 7.5 μM, PIFP triggers the aggregation of lipid vesicles, increasing the particle size detected in solution. Taking the upper-bound PIFP CAC as 7.5 μM yields an approximate maximum ratio of 1 peptide to 20 anionic lipids in the system; this represents an overall balanced charge of −15, which is still far for an electrostatic neutralization hypothesis. Considering all of the data presented so far, it is most likely that PIFP aggregation triggering and simultaneous fusion mechanisms are dependent on a membrane-surface-controlled oligomerization and consequent pore formation. However, this hypothesis is hard to prove *in vitro*. For this reason, an *in silico* analysis of the PIFP−membrane interactions were performed.

CG Simulations Reveal the PIFP Aggregates When Inside a POPC:POPG Membrane. To complement the data obtained experimentally and to better understand what occurs at a molecular level upon PIFP insertion in the membrane, we performed CG and AA MD simulations.

First, CG simulations of PIFP in a membrane bilayer were performed to understand how the PIFP assembles and latter convert it to atomistic detail to analyze the molecular interactions that stabilize it. Only a mixed bilayer composed of POPC:POPG (4:1) was studied since the data we obtained for the PIFP−lipid fusion induction showed that this peptide has virtually no activity in pure POPC membranes (Figure 2A).

To study the influence of different peptide concentrations, we built four MARTINI 3[40] CG systems with increasing peptide/lipid concentrations and simulated each one for 20 μs. The detailed composition of the systems is shown in those tested experimentally, and a snapshot of these systems can be seen in Figure S1.

When performing preliminary short simulations of these systems, we observed that, when inserted vertically in the membrane, the peptides would come to the top of the outer leaflet. Since previous NMR data shows that the PIFP adopts a membrane-spanning conformation when interacting with POPC:POPG (4:1) membranes,[30] we applied a flat-bottomed harmonic well potential in all systems to ensure that the peptide would remain vertically inserted in the membrane. It is worth noting that, further on, when converting these CG systems to AA, the peptides were able to remain vertically inserted in the membrane without needing any restraints. Moreover, our objective was not to assess the peptide
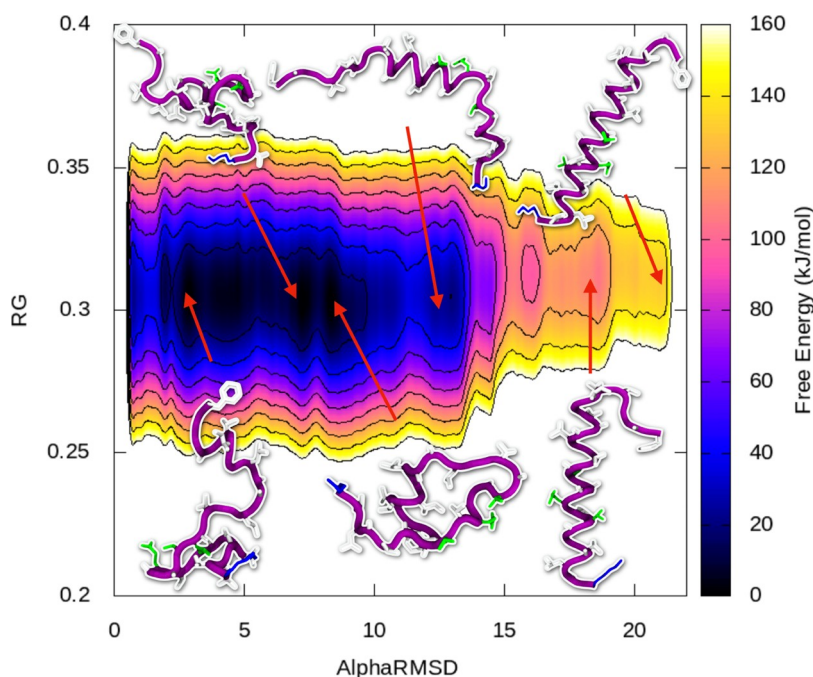
Figure 4. Free-energy surface of the PIFP in water obtained from Metadynamics calculations. A two-dimensional (2D) free-energy landscape was built as a function of the CVs AlphaRMSD and radius of gyration (RG). The free energy was reconstructed from the bias potential, and contour lines are used to represent regions with identical free-energy values. Structures corresponding to the most relevant basins are illustrated using molecular images built with VMD[51] using the same color scheme as in Figure 1C.

orientation in the membrane, which was already known, but rather to determine how the peptides assemble and interact with each other in the membrane. Thus, we used the experimental findings regarding the PIFP orientation in the membrane to guide the simulations and reduce the degrees of freedom of the system.

After 20 μs of CG simulation, we saw that, in all of the systems with multiple peptides, these interacted to form oligomeric structures (as shown in the molecular images in Figure 3). Visual inspection of the trajectories revealed that these contacts were fairly persistent; i.e., after the first contact between any two peptides, the interaction was maintained throughout the simulation. The concentration-dependent peptide−peptide and/or peptide−lipid aggregation observed when performing a PIFP−lipid binding analysis also reinforces this observation (Figure 3).

The PIFPs stayed inside the membrane throughout the simulation, as seen in Figure 3, which indicates that the flat-bottom restraint applied was sufficient to recreate the experimentally observed orientation. In terms of peptide-induced membrane effects, we saw that, for the system with the highest peptide/lipid ratio (nine peptides), there is a tendency for the membrane leaflets to come close to each other. This is clear in Figure 3D where there is a very slight decrease in the membrane thickness due to small membrane deformations better seen in the zoomed-in inset.

Membrane hydration increases with increasing PIFP concentrations. For the two systems with the highest PIFP concentrations, waters can penetrate deeper than the lipid headgroups and reach the membrane core (Figure 3C,D), which might be facilitated by the peptide aggregation mentioned above.

A common effect of the addition of FPs to a membrane is the increase[19−21] or decrease in the lipid tail order.[22,23] To measure the membrane disturbance induced by these peptides

on the membrane, we determined the lipid order parameters in all four CG simulations (Figure S2). These results showed that lipid tail order decreases with increasing peptide concentrations.

The behavior seen in the CG simulations is in agreement with what was seen experimentally, showing not only that these peptides tend to aggregate when inside a membrane[14] but also that these clusters facilitate the entry of water molecules to its core.[31]

PIFP That Can Adopt Moderately Helical Structures in Water and Helicity in the Membrane Is Influenced by the Peptide/Lipid Ratio. During the fusion process, the F protein suffers conformational changes and, before inserting into the membrane, the PIFP becomes exposed to water. To characterize the peptide's structural properties in aqueous solution, we performed metadynamics simulations and, in line with the CD results, the PIFP is mainly a random coil in aqueous solution, but it has a heterogeneous energy landscape and can easily adopt moderately helical structures (Figure 4). This can facilitate its transition into the helical structure that it adopts in the membrane.

To analyze the PIFP secondary structure in the membrane with atomistic detail, we converted the final systems of the CG simulations to AA resolution. Triplicates of all four systems were simulated for 1 μs without any restraints. The analysis of the peptide's secondary structure in a POPC:POPG membrane revealed that at low peptide/lipid ratio (1 peptide copy) the peptide maintained its helical conformation losing it only at the N- and C-terminal ends (Figure 5A). For the other three systems, there was also the loss of structure at both ends, with the N-terminus being the most impacted (Figure 5B−D). In the system with three peptides, the first two N-terminal residues lose entirely their helical structure, in all replicates. In the hexamer, the loss of helicity affects five N-terminal residues, and in the nonamer, six residues are affected. The
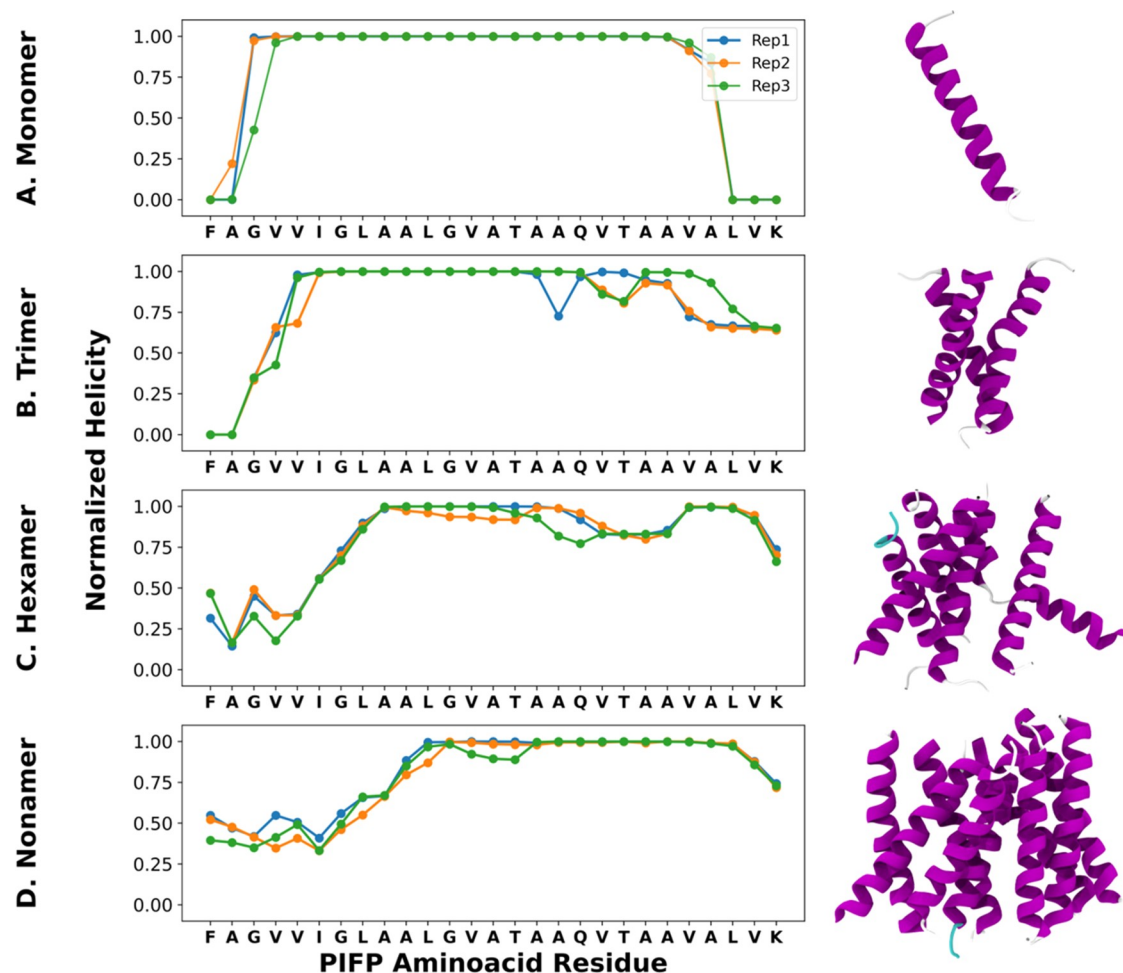
Figure 5. PIFP dynamic helicity during atomistic MD simulations. The plots show the average helicity values obtained for each residue in each of three replicate 1 μs long MD simulations using the GROMACS tool gmx do_dssp[52] (data for each replicate is shown in a different color). The images to the right are snapshots of the simulation with the helix motifs highlighted in purple.

loss of structure seen in these regions may be due to the passage of water molecules into the porelike structures and consequent increase in the number of PIFP−water contacts in this region (Figure S4). This is in line with the results seen in metadynamics simulations and CD analysis, which shows that the peptide's structure is destabilized in the aqueous environment. Concurrently, in the six-copy system, there is additional loss of α-helical structure at residues T117, A118, A119, and Q120. This is the same region where a bend, with its vertex at T117, is found in the prefusion crystal structure of the parainfluenza fusion protein,[41,42] indicating that this region might be flexible.

When looking at the interpeptide contacts between residues (those within 4.5 Å; Figure 6), these are prevalent in the C-terminal region of the trimer, unlike the N-terminal region, where no interpeptide contacts are seen (Figure 6A). A different behavior is seen in the systems with higher PIFP concentrations, where both terminals have peptide−peptide contacts (Figure 6B,C). The prevalence of these contacts in the N-terminal region increases from the hexamer to the nonamer but they are always less frequent than in the C-terminal region.

The regions of the PIFPs, where low percentages of interpeptide contacts were identified, also form stable interactions with the membrane lipids (Figure S5), guarantee-

ing the stability of the oligomeric structures in the membrane. When analyzing the interactions between the PIFPs and the PG lipid heads, the N-terminal region—that is predicted to insert all the way through the membrane—is the one with the most contacts (Figure S6). This is compatible with the fact that, in the plasma membrane, the negatively charged lipids are found in the inner layer of the membrane and, consequently, only the N-terminal region of the peptide would be able to interact with these lipid heads.

Since peptide bending has been described as an important FP feature to induce membrane disturbance and consequent reduction of the energetic barrier for membrane fusion,[43,44] we analyzed if the PIFP forms the same bend inside this membrane bilayer (Figure S7). The helix geometry analysis showed that in one replicate of the hexameric system there is increased departure from a straight helix (represented in Figure S7 by helix bending angles farther from 180°), supporting that the local loss of helicity around T117 is induced by an increase in peptide curvature.

Overall, there seems to be a correlation between the number of copies of the PIFP and the loss of α-helical structure. This observation is in good agreement with the data we obtained by CD (Figure 2D) and previous NMR structural analysis.[30] Both the CD and NMR experiments[30] showed that at low peptide/lipid ratios, in a POPC:POPG membrane, the peptide has an
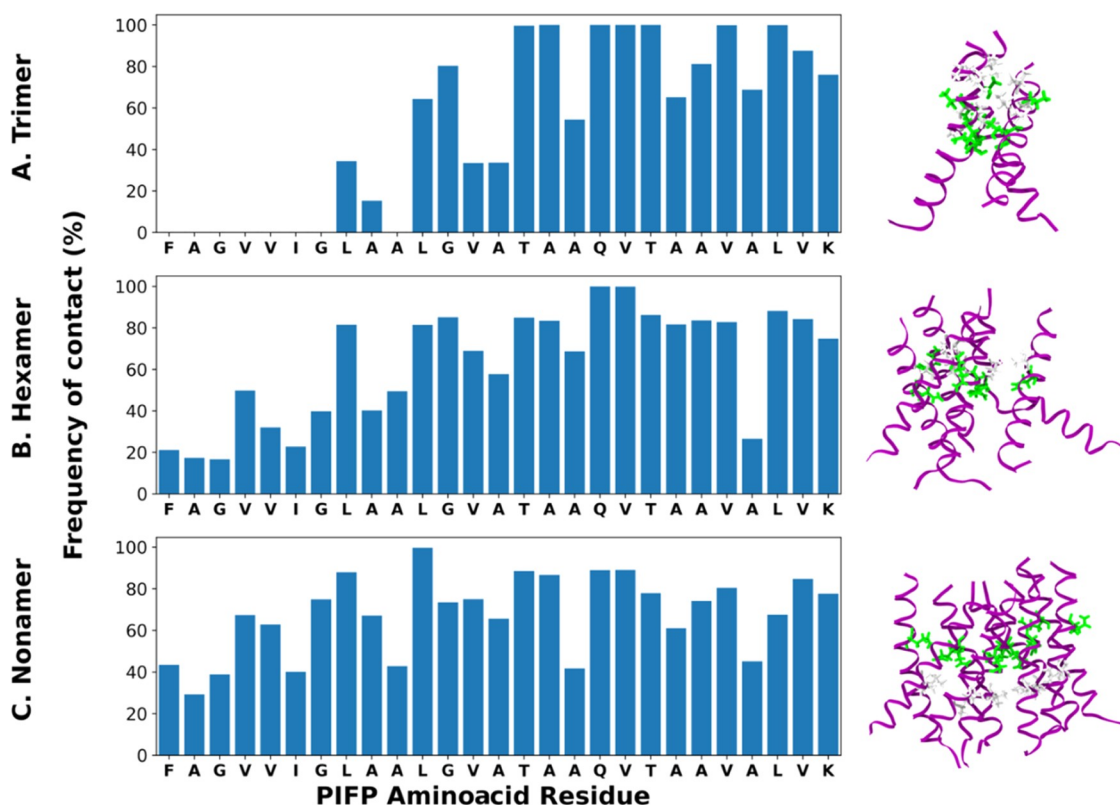
Figure 6. Prevalence of peptide–peptide contacts. The plots show the prevalence of contacts between different peptides, within 4.5 Å, established by each amino acid residue, and averaged over the simulation. This analysis was only performed for the systems with more than one peptide. Each plot has to its right a snapshot of the final frame of the corresponding simulation, where the PIFPs are shown in purple and the residues involved in the peptide–peptide contacts with a prevalence higher than 90% are highlighted in green (polar residues) and white (nonpolar residues).

α-helical structure, and at higher ratios, our CD data shows that the helical structure is less well defined (Figure 2D, gray line).

Finally, we hypothesize that at low PIFP concentrations the peptide maintains its α-helical structure due to the hydrophobic environment inside the membrane, losing its structure only in the terminal regions (more exposed to water). With the increase in the number of copies of the PIFP, there is a loss of structure due to the formation of prevalent interpeptide interactions.

PIFP Peptide–Peptide Interactions Stabilize Porelike Structures. As mentioned earlier, during the membrane fusion process, after binding to the target cell, conformational changes occur in the F protein leading to its trimerization, and at least two parainfluenza F protein trimers are necessary for the viral fusion process to occur.[8−10] This means that at least six fusion peptides are involved in the fusion process.

To determine if there is a specific contact region between the PIFPs, we analyzed the data obtained for the peptide–peptide contacts occurring between residues of different peptides (Figure 6) and determined the accessibility of water to the core of the membrane (Figure 7A−C).

Through the contact analysis, we saw that, in the systems with more than one peptide, the residues forming more prevalent contacts were those with hydrophobic side chains (L110, L113, A118, V121, V125, and L127) and the polar residues (T117, Q120, and T122).

Additionally, in the trimeric PIFP, there is 100% of prevalence of contacts involving residues T117, A118, Q120, V121, and T122, all located in the C-terminal region of the

PIFP. These contacts create a specific surface of contact stabilizing this end of the structure (Figure 6A, molecular image). This is also the region where the HOLE2 tool found the space for the entry of water molecules (Figure 7A), but the inexistence of interpeptide interactions at the other end (the N-terminal region) prevents the formation of a viable pore.

In the hexamer, contacts involving Q120 and V121 residues are maintained throughout the simulation, but, unlike the trimer, N-terminal residues form transient contacts (with a prevalence of around 20%) that stabilize the transmembrane structure enough to create just enough space for the passage of water through the membrane (Figure 7B).

Finally, in the nonamer, even though interpeptide interactions are less prevalent, they are more vertically distributed. Contacts with L113 are seen all throughout the simulation, and the contacts at the N-terminal have an incidence close to 40%. Similarly to the trimer and hexamer, the N-terminal region has a relatively low interpeptide contact incidence, which we found interesting given that several hyperfusogenic mutations occur in this region.[45] The effect of these point mutations on the peptide–peptide clustering, and consequently on the PIFP fusion, should be addressed in future studies. Nonetheless, the formation of several interpeptide contacts within the nonamers' PIFPs forms a wide water-accessible region inside the membrane and, consequently, the ideal conformation for the formation of a porelike structure (Figure 7C).

Looking at RMSD data of the nonamer (Figure S8—4th row), there is a significant deviation in peptide 4 of replicate 3. Superimposing the last frames of the CG and AA simulations,
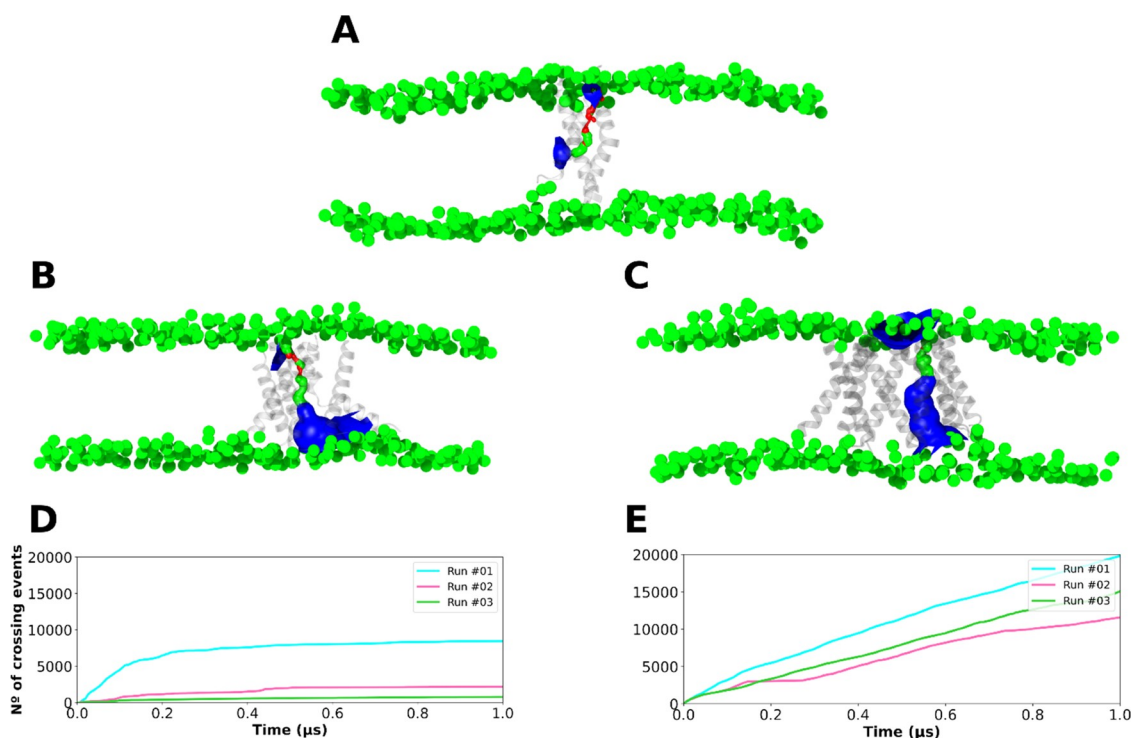
Figure 7. PIFP pore characterization. Panels (A−C) are figures generated by the HOLE2 analysis tool from MD analysis that show the accessibility of water to the membrane for the trimeric, hexameric, and nonameric systems, respectively. The parts that are inaccessible to water (pore radius < 1.15 Å) are shown in red, water-accessible parts (1.15 Å < pore radius < 2.30 Å) are shown in green, and wide areas (pore radius > 2.30 Å) are displayed in blue. Panels (D) and (E) show the number of water-crossing events that were determined for the systems with six and nine PIFPs, respectively.

considerable changes in conformation and bending of peptide 4 are clear (Figure S9—peptide in red). However, the impact on the overall structure of the porelike structure and water penetration is identical when comparing AA and CG simulations (Figure S4).

These results show that the increase in the PIFP concentration facilitates the formation of peptide−peptide interactions between the PIFP's hydrophobic and polar residues and that these stable interactions are of utmost importance for the assembly of porelike structures inside the membrane. Additionally, the formation of these structures in our simulations can explain the increased vesicle leakage seen experimentally at high peptide/lipid concentrations (Figure 2B).

Water Can Pass through the PIFP Porelike Structures. To determine if the previous porelike structures enable the passage of water, thus explaining the PIFP-induced leakage of 5,6-CF-loaded vesicles seen experimentally (Figure 2B), we analyzed the accessibility of water to the core of the membrane and the flux of water molecules through the pores. For the latter, we used the fluxer[46] script, which counts the number of crossing events across a finite thickness xy-plane membrane.

The results showed that both systems form pores that are vehicles for the passage of water molecules through the membrane (Figure 7D,E). In the system with six peptides, the flux analysis showed that there is a positive flux of water until approximately 200 ns of simulation (in replicate 1). At this point, the flux is slowed/stopped (the slope of the line becomes close to 0). An explanation for the abrupt deceleration seen in the water flow can be the partial closing of the pore in this replicate. For replicates 2 and 3, the

cumulative flux is lower but continuous; this suggests that in these replicates there is no initial open state (Figure 7D).

For the nonamer, the flux of water inside the pore is continuous in all replicates. The water flux is initially identical in all three replicates, but different peptide rearrangements in each replicate then lead to some divergence. From 500 ns of simulation onward, the flux becomes again approximately the same for all three replicates (Figure 7E).

A density analysis of the position of lipid heads and water molecules during the simulations was also performed (Figures S5 and S6, respectively), with results consistent with the passage of water through the core of the membrane. First, when looking at the lipid head density data for the two systems with the highest peptide concentration (from the top view), we see an opening on both sides of the membrane (Figure S10C,D). The absence of lipid heads in this area is an indication that the oligomeric structures can form a stable peptide arrangement that removes the lipids from this central area. In this same region, by analyzing the water density data, we can see that it is common to find water molecules (in blue) in the core of the membrane (in white) (Figure S11C,D).

Overall, we saw that at higher peptide concentrations there is a continuous flux of water through the membrane due to the formation of a stable oligomeric PIFP structure that, despite not being a requirement for membrane fusion, is a sign of strong PIFP-induced membrane disturbance. This flux of water through the membrane explains the experimental PIFP-induced leakage observed at higher PIFP concentrations (Figure 2B).

PIFP Induces Concentration-Dependent Lipid Tail Protrusion. It is known that to promote membrane fusion, the FPs must perturb the properties of fluid lipid bilayers.
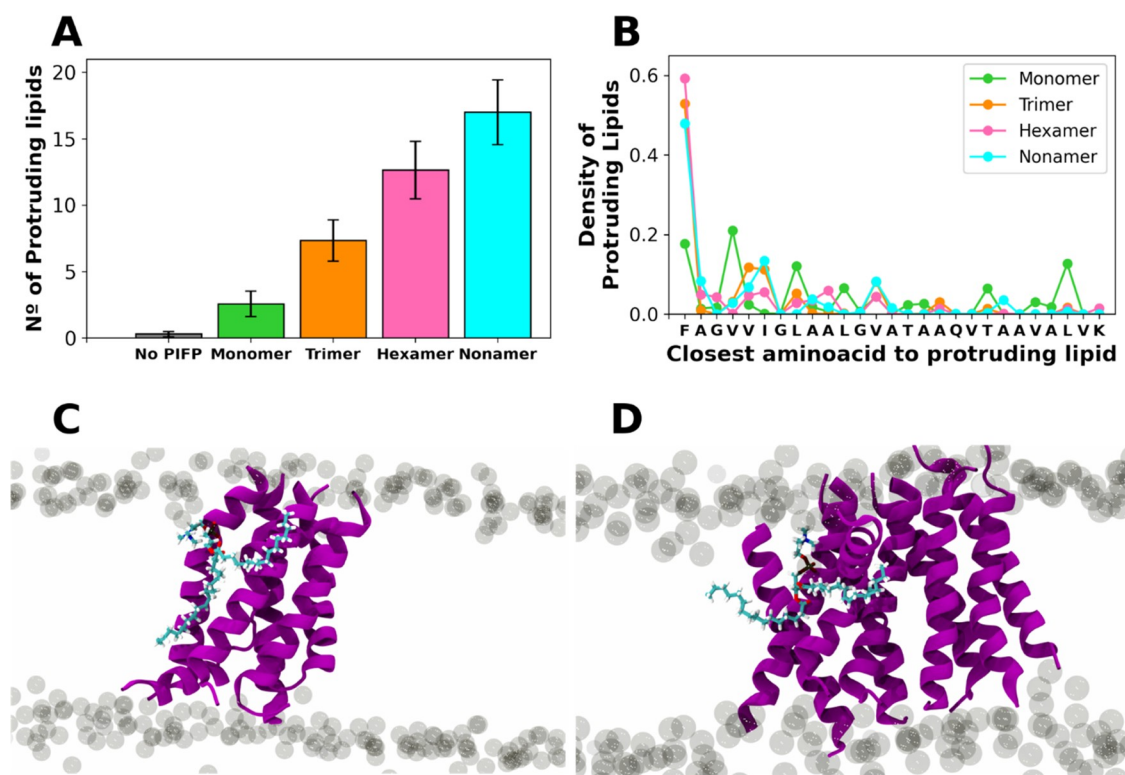
Figure 8. Lipid tail protrusion. (A) The plot shows the average number of protruding lipids at 4 Å from the peptides. A pure membrane (no PIFP) was used as a reference for the lipids that protrude without the influence of peptides. Error bars represent the 95% confidence intervals and were calculated with bootstrap resampling. Plot (B) shows the amino acid residues that are closest to a protruding lipid. Panels (C) and (D) are snapshots of the hexameric and nonameric simulations, respectively, where a lipid is highlighted in blue to evidence the lipid tail protrusion event.

Effects induced by the FPs can be the induction of spontaneous curvature, hydration, changes in acyl chain order,[47] or promotion of lipid tail protrusion.

To measure the membrane disturbance induced by the increasing concentrations of peptide, we determined the order parameters, the number of membrane lipid tail protrusion events, and peptide−lipid contacts occurring during the simulations.

The lipid order values were obtained by averaging the S-values for each acyl chain carbon of the lipid tails over time and were calculated for the lipids in a pure membrane (without peptides, as a control) and with the peptides (Figure S12). Slightly higher S-values were obtained in the presence of the PIFPs—especially in the nonamer, whereas the monomer S-values are practically the same as the control's (Figure S12A). The order behavior is the same when looking only at the lipids closest to the peptides (within 5 Å; Figure S12B).

Another mechanism that has been proposed to explain the FP-induced membrane fusion is the promotion of lipid tail protrusion events. These were first described based on MD data and correspond to the outward extension of lipid acyl chains, beyond the corresponding phosphate group, facilitating the fusion between opposite membranes[22,24,26,27,48] (Figure 8C,D). We also observed this when simulating the influenza FP in a membrane bilayer.[22,27,48]

The lipid tail protrusion results showed that there is a gradual increase in the number of protruding lipids when the number of simulated peptides increases: monomer < trimer < hexamer < nonamer (Figure 8A). This increase in the peptide/lipid ratios leads to a linear increase in the number of protruding lipids, which precludes the occurrence of

synergistic. We also analyzed which residues were closest to the protruding lipids (Figure 8B) and, as is the case for other FPs, the N-terminal residues[22,26−28] seem to be those inducing the most lipid protrusion events. The N-terminal phenylalanine residue seems to play a key role in the induction of headgroup intrusions (the lipid headgroup penetrates deeper into the membrane)[22,26−28] (Figure S10), an event that facilitates the occurrence of lipid tail protrusion events. Peptide−lipid contact analysis also shows that the N-terminal region of the trimer and hexamer interacts preferentially with POPG lipids (Figure S5) and, on average, these oligomeric PIPFs contact with POPG lipids 1.5 more times than with POPC (Figure S13). Interestingly, the results indicate that oligomerization facilitates the N-ter:POPG interactions since the interaction is much less frequent in the monomer than in the systems with multiple peptides.

Lipid head density analysis shows that for the systems with higher peptide concentrations, it is common to find the lipid heads inside of the membrane (Figure S10C,D). This is consistent with the notion that the N-terminal residues of the PIFP interact with the lipid heads, inducing lipid head intrusion that, in turn, facilitates the protrusion of the corresponding tails.

These results show that the PIFP induces lipid tail protrusion that increases with the concentration of peptide. This is in very good agreement with the peptide-induced lipid mixing data, which show a similar trend: at higher peptide concentrations, there is more lipid mixing (Figure 1A, right panel).

DISCUSSION

The aim of this work was to characterize the mechanisms of membrane fusion that occur during parainfluenza infection. With this in mind, we performed CG and atomistic molecular dynamics (MD) simulations, together with spectroscopic experiments of the PIFP in a POPC:POPG (with a ratio of 4:1) lipid bilayer. An important aspect that remained unclear is the effect of concentration/oligomerization of the PIFP. We addressed this question by performing a thorough computational and experimental characterization of systems with increasing peptide/lipid ratios.

Experimental CD results showed that, upon interaction with membranes, the PIFP evolves from a random-coil conformation in solution to an α-helical conformation. Metadynamics simulations revealed that, although the peptide is mainly unstructured in water, it can adopt moderately helical structures, which might facilitate the acquisition of a helical structure upon membrane interaction. The concentration-dependent behavior of the secondary structure in the membrane was also seen in the AA MD simulations where the PIFP structure is α-helical at low PIFP concentrations, with some structure loss seen when increasing the peptide concentration. This is likely due to the formation of polar and hydrophobic contacts between the peptides, which lead to the formation of oligomeric structures.

The formation of these oligomeric structures explains the 5,6-CF leakage increase at higher PIFP concentrations. In fact, when analyzing the peptide−membrane interactions, the simulation results show that with higher peptide concentrations the oligomeric structures form porelike structures that facilitate the flux of water through the membrane.

Although the PIFP had been suggested to form a fusion pore,[31] this is the first time that it is shown to spontaneously assemble into oligomeric structures that induce the formation of a water-permeable pore. Moreover, the computational analyses reveal that these peptides can induce lipid protrusion events without greatly altering the lipid order. This is in line with what has been observed for other FPs[22,23,27,28,48] and indicates that lipid tail protrusion plays an important role in viral membrane fusion (see Lousa and Soares[49] for a review that discusses this topic).

The results obtained complement the previous experimental studies and strongly support the hypothesis that the FP promotes membrane fusion by destabilizing the host membrane, a role that is better fulfilled at higher peptide concentrations. Even though in our *in silico* studies both the hexameric and nonameric conformations play an essential role in the membrane destabilization, *in vitro* studies revealed that, when in phospholipid micelles, the PIFP assembles preferably into hexamers.[31]

Interestingly, the effect of this peptide on the membrane, namely, the induction of lipid tail protrusion[23,27,28,48] and the entry of waters to the core of the membrane when the peptides are transmembrane,[50] is similar to that observed for the influenza fusion peptide, supporting the hypothesis that fusion peptides from different viruses share common mechanisms. These findings provide a valuable contribution to the advance of the knowledge on viral fusion peptides, which, given their importance, can be very useful for the development of antiviral therapies.

ASSOCIATED CONTENT

Ⓢⓘ Supporting Information

The Supporting Information is available free of charge at https://pubs.acs.org/doi/10.1021/acschembio.2c00208.

> Extended materials provide the materials and methods, additional snapshots of the initial CG system and analysis results on lipid order parameters, PIFP helix geometry, water densities, phospholipid head densities, RMSD, and RMSF (PDF)

AUTHOR INFORMATION

Corresponding Authors

Cláudio M. Soares − *Instituto de Tecnologia Química e Biológica, Universidade Nova de Lisboa, 2780-157 Oeiras, Portugal*; Email: claudio@itqb.unl.pt

Ana Salomé Veiga − *Instituto de Medicina Molecular, Faculdade de Medicina da Universidade de Lisboa, 1649-028 Lisboa, Portugal*; ⓞ orcid.org/0000-0002-9892-2243; Email: aveiga@medicina.ulisboa.pt

Diana Lousa − *Instituto de Tecnologia Química e Biológica, Universidade Nova de Lisboa, 2780-157 Oeiras, Portugal*; ⓞ orcid.org/0000-0002-2309-0980; Email: dlousa@itqb.unl.pt

Authors

Mariana Valério − *Instituto de Tecnologia Química e Biológica, Universidade Nova de Lisboa, 2780-157 Oeiras, Portugal*; ⓞ orcid.org/0000-0001-7340-0134

Diogo A. Mendonça − *Instituto de Medicina Molecular, Faculdade de Medicina da Universidade de Lisboa, 1649-028 Lisboa, Portugal*; ⓞ orcid.org/0000-0001-8003-4662

João Morais − *Instituto de Medicina Molecular, Faculdade de Medicina da Universidade de Lisboa, 1649-028 Lisboa, Portugal*

Carolina C. Buga − *Instituto de Tecnologia Química e Biológica, Universidade Nova de Lisboa, 2780-157 Oeiras, Portugal; Instituto de Medicina Molecular, Faculdade de Medicina da Universidade de Lisboa, 1649-028 Lisboa, Portugal*; ⓞ orcid.org/0000-0003-4109-8502

Carlos H. Cruz − *Instituto de Tecnologia Química e Biológica, Universidade Nova de Lisboa, 2780-157 Oeiras, Portugal*

Miguel A.R.B. Castanho − *Instituto de Medicina Molecular, Faculdade de Medicina da Universidade de Lisboa, 1649-028 Lisboa, Portugal*; ⓞ orcid.org/0000-0001-7891-7562

Manuel N. Melo − *Instituto de Tecnologia Química e Biológica, Universidade Nova de Lisboa, 2780-157 Oeiras, Portugal*; ⓞ orcid.org/0000-0001-6567-0513

Complete contact information is available at:
https://pubs.acs.org/10.1021/acschembio.2c00208

Author Contributions

§M.V. and D.A.M. contributed equally to this work. M.V., C.H.C., M.N.M., C.M.S., and D.L. designed the computational systems and analysis and M.V. and C.H.C performed them. D.A.M., J.M., C.C.B., M.A.R.B.C., and A.S.V. designed the experimental assays and D.A.M., J.M., and C.C.B. performed the experiments. All authors contributed to manuscript writing and revision and have given approval to the final version of the manuscript.

Notes

The authors declare no competing financial interest.

■ REFERENCES

(1) Chang, A.; Dutch, R. E. Paramyxovirus Fusion and Entry: Multiple Paths to a Common End. *Viruses* **2012**, *4*, 613−636.

(2) Dutch, R. E. Entry and Fusion of Emerging Paramyxoviruses. *PLoS Pathog.* **2010**, *6*, No. e1000881.

(3) Abedi, G. R.; Prill, M. M.; Langley, G. E.; Wikswo, M. E.; Weinberg, G. A.; Curns, A. T.; Schneider, E. Estimates of Parainfluenza Virus-Associated Hospitalizations and Cost Among Children Aged Less Than 5 Years in the United States, 1998−2010. *J. Pediatr. Infect. Dis. Soc.* **2016**, *5*, 7−13.

(4) Lamb, R. A.; Parks, G. D. Paramyxoviridae. In *Fields Virology: Sixth Edition*; Wolters Kluwer Health Adis (ESP), 2013.

(5) Skehel, J. J.; Wiley, D. C. Receptor Binding and Membrane Fusion in Virus Entry: The Influenza Hemagglutinin. *Annu. Rev. Biochem.* **2000**, *69*, 531−569.

(6) Lamb, R. A. Paramyxovirus Fusion: A Hypothesis for Changes. *Virology* **1993**, *197*, 1−11.

(7) Russell, C. J.; Jardetzky, T. S.; Lamb, R. A. Membrane Fusion Machines of Paramyxoviruses: Capture of Intermediates of Fusion. *EMBO J.* **2001**, *20*, 4024−4034.

(8) Hernandez, L. D.; Hoffman, L.; Wolfsberg, T.; White, J. Virus-Cell and Cell-Cell Fusion. *Annu. Rev. Cell Dev. Biol.* **1996**, *12*, 627−661.

(9) Baker, K. A.; Dutch, R. E.; Lamb, R. A.; Jardetzky, T. S. Structural Basis for Paramyxovirus-Mediated Membrane Fusion. *Mol. Cell* **1999**, *3*, 309−319.

(10) Eckert, D. M.; Kim, P. S. Mechanisms of Viral Membrane Fusion and Its Inhibition. *Annu. Rev. Biochem.* **2001**, *70*, 777−810.

(11) Horvath, C. M.; Lamb, R. A. Studies on the Fusion Peptide of a Paramyxovirus Fusion Glycoprotein: Roles of Conserved Residues in Cell Fusion. *J. Virol.* **1992**, *66*, 2443−2455.

(12) Russ, W. P.; Engelman, D. M. The GxxxG Motif: A Framework for Transmembrane Helix-Helix Association. *J. Mol. Biol.* **2000**, *296*, 911−919.

(13) Kleiger, G.; Grothe, R.; Mallick, P.; Eisenberg, D. GXXXG and AXXXA: Common α-Helical Interaction Motifs in Proteins, Particularly in Extremophiles. *Biochemistry* **2002**, *41*, 5990−5997.

(14) Bagai, S.; Lamb, R. A. A Glycine to Alanine Substitution in the Paramyxovirus SV5 Fusion Peptide Increases the Initial Rate of Fusion. *Virology* **1997**, *238*, 283−290.

(15) Pattnaik, G. P.; Meher, G.; Chakraborty, H. Exploring the Mechanism of Viral Peptide-Induced Membrane Fusion. In *Biochemical and Biophysical Roles of Cell Surface Molecules*; Springer, 2018; pp 69−78.

(16) Lagüe, P.; Roux, B.; Pastor, R. W. Molecular Dynamics Simulations of the Influenza Hemagglutinin Fusion Peptide in Micelles and Bilayers: Conformational Analysis of Peptide and Lipids. *J. Mol. Biol.* **2005**, *354*, 1129−1141.

(17) Collu, F.; Spiga, E.; Lorenz, C. D.; Fraternali, F. Assembly of Influenza Hemagglutinin Fusion Peptides in a Phospholipid Bilayer by Coarse-Grained Computer Simulations. *Front. Mol. Biosci.* **2015**, *2*, No. 66.

(18) Fuhrmans, M.; Marrink, S. J. Molecular View of the Role of Fusion Peptides in Promoting Positive Membrane Curvature. *J. Am. Chem. Soc.* **2012**, *134*, 1543−1552.

(19) Lai, A. L.; Freed, J. H. HIV Gp41 Fusion Peptide Increases Membrane Ordering in a Cholesterol-Dependent Fashion. *Biophys. J.* **2014**, *106*, 172−181.

(20) Meher, G.; Chakraborty, H. Membrane Composition Modulates Fusion by Altering Membrane Properties and Fusion Peptide Structure. *J. Membr. Biol.* **2019**, *252*, 261−272.

(21) Chakraborty, H.; Lentz, B. R.; Kombrabail, M.; Krishnamoorthy, G.; Chattopadhyay, A. Depth-Dependent Membrane Ordering by Hemagglutinin Fusion Peptide Promotes Fusion. *J. Phys. Chem. B* **2017**, *121*, 1640−1648.

(22) Victor, B. L.; Lousa, D.; Antunes, J. M.; Soares, C. M. Self-Assembly Molecular Dynamics Simulations Shed Light into the Interaction of the Influenza Fusion Peptide with a Membrane Bilayer. *J. Chem. Inf. Model.* **2015**, *55*, 795−805.

(23) Larsson, P.; Kasson, P. M. Lipid Tail Protrusion in Simulations Predicts Fusogenic Activity of Influenza Fusion Peptide Mutants and Conformational Models. *PLoS Comput. Biol.* **2013**, *9*, No. e1002950.

(24) Kasson, P. M.; Lindahl, E.; Pande, V. S. Atomic-Resolution Simulations Predict a Transition State for Vesicle Fusion Defined by Contact of a Few Lipid Tails. *PLoS Comput. Biol.* **2010**, *6*, No. e1000829.

(25) Risselada, H. J.; Marelli, G.; Fuhrmans, M.; Smirnova, Y. G.; Grubmüller, H.; Marrink, S. J.; Müller, M. Line-Tension Controlled Mechanism for Influenza Fusion. *PLoS One* **2012**, *7*, No. e38302.

(26) Légaré, S.; Lagüe, P. The Influenza Fusion Peptide Promotes Lipid Polar Head Intrusion through Hydrogen Bonding with Phosphates and N-Terminal Membrane Insertion Depth. *Proteins* **2014**, *82*, 2118−2127.

(27) Lousa, D.; Pinto, A. R.; Victor, B. L.; Laio, A.; Veiga, A. S.; Castanho, M. A.; Soares, C. M. Fusing Simulation and Experiment: The Effect of Mutations on the Structure and Activity of the Influenza Fusion Peptide. *Sci. Rep.* **2016**, *6*, No. 28099.

(28) Pabis, A.; Rawle, R. J.; Kasson, P. M. Influenza Hemagglutinin Drives Viral Entry via Two Sequential Intramembrane Mechanisms. *Proc. Natl. Acad. Sci. U.S.A.* **2020**, *117*, 7200−7207.

(29) Holt, A.; Killian, J. A. Orientation and Dynamics of Transmembrane Peptides: The Power of Simple Models. *Eur. Biophys. J.* **2010**, *39*, 609−621.

(30) Yao, H.; Hong, M. Conformation and Lipid Interaction of the Fusion Peptide of the Paramyxovirus PIV5 in Anionic and Negative-Curvature Membranes from Solid-State NMR. *J. Am. Chem. Soc.* **2014**, *136*, 2611−2624.

(31) Donald, J. E.; Zhang, Y.; Fiorin, G.; Carnevale, V.; Slochower, D. R.; Gai, F.; Klein, M. L.; DeGrado, W. F. Transmembrane Orientation and Possible Role of the Fusogenic Peptide from Parainfluenza Virus 5 (PIV5) in Promoting Fusion. *Proc. Natl. Acad. Sci. U.S.A.* **2011**, *108*, 3958−3963.

(32) Maier, O.; Oberle, V.; Hoekstra, D. Fluorescent Lipid Probes: Some Properties and Applications (a Review). *Chem. Phys. Lipids* **2002**, *116*, 3−18.

(33) Basso, L. G. M.; Vicente, E. F.; Crusca, E.; Cilli, E. M.; Costa-Filho, A. J. SARS-CoV Fusion Peptides Induce Membrane Surface Ordering and Curvature. *Sci. Rep.* **2016**, *6*, No. 37131.

(34) Epand, R. M. Fusion Peptides and the Mechanism of Viral Fusion. *Biochim. Biophys. Acta, Biomembr.* **2003**, *1614*, 116−121.

(35) Figueira, T. N.; Freire, J. M.; Cunha-Santos, C.; Heras, M.; Gonçalves, J.; Moscona, A.; Porotto, M.; Salomé Veiga, A.; Castanho, M. A. R. B. Quantitative Analysis of Molecular Partition towards Lipid Membranes Using Surface Plasmon Resonance. *Sci. Rep.* **2017**, *7*, No. 45647.

(36) Santos, N. C.; Prieto, M.; Castanho, M. A. R. B. Interaction of the Major Epitope Region of HIV Protein Gp41 with Membrane Model Systems. A Fluorescence Spectroscopy Study. *Biochemistry* **1998**, *37*, 8674−8682.

(37) Santos, N. C.; Prieto, M.; Castanho, M. A. R. B. Quantifying Molecular Partition into Model Systems of Biomembranes: An Emphasis on Optical Spectroscopic Methods. *Biochim. Biophys. Acta, Biomembr.* **2003**, *1612*, 123−135.

(38) Xia, Y.; Sun, J.; Liang, D. Aggregation, Fusion, and Leakage of Liposomes Induced by Peptides. *Langmuir* **2014**, *30*, 7334−7342.

(39) Nir, S.; Nicol, F.; Szoka, F. C. Surface Aggregation and Membrane Penetration by Peptides: Relation to Pore Formation and Fusion. *Mol. Membr. Biol.* **1999**, *16*, 95−101.

(40) Souza, P. C. T.; Alessandri, R.; Barnoud, J.; Thallmair, S.; Faustino, I.; Grünewald, F.; Patmanidis, I.; Abdizadeh, H.; Bruininks, B. M. H.; et al. Martini 3: A General Purpose Force Field for Coarse-Grained Molecular Dynamics. *Nat. Methods* **2021**, *18*, 382−388.

(41) Yin, H.-S.; Wen, X.; Paterson, R. G.; Lamb, R. A.; Jardetzky, T. S. Structure of the Parainfluenza Virus 5 F Protein in Its Metastable, Prefusion Conformation. *Nature* **2006**, *439*, 38−44.

(42) Welch, B. D.; Liu, Y.; Kors, C. A.; Leser, G. P.; Jardetzky, T. S.; Lamb, R. A. Structure of the Cleavage-Activated Prefusion Form of the Parainfluenza Virus 5 Fusion Protein. *Proc. Natl. Acad. Sci. U.S.A.* **2012**, *109*, 16672−16677.

(43) Lai, A. L.; Tamm, L. K. Locking the Kink in the Influenza Hemagglutinin Fusion Domain Structure*. *J. Biol. Chem.* **2007**, *282*, 23946−23956.

(44) Légaré, S.; Lagüe, P. The Influenza Fusion Peptide Adopts a Flexible Flat V Conformation in Membranes. *Biophys. J.* **2012**, *102*, 2270−2278.

(45) Johnson, J. B.; Schmitt, A. P.; Parks, G. D. Point Mutations in the Paramyxovirus F Protein That Enhance Fusion Activity Shift the Mechanism of Complement-Mediated Virus Neutralization. *J. Virol.* **2013**, *87*, 9250−9259.

(46) Melo, M. N.; Arnarez, C.; Sikkema, H.; Kumar, N.; Walko, M.; Berendsen, H. J. C.; Kocer, A.; Marrink, S. J.; Ingólfsson, H. I. High-Throughput Simulations Reveal Membrane-Mediated Effects of Alcohols on MscL Gating. *J. Am. Chem. Soc.* **2017**, *139*, 2664−2671.

(47) Tamm, L. K.; Han, X. Viral Fusion Peptides: A Tool Set to Disrupt and Connect Biological Membranes. *Biosci. Rep.* **2000**, *20*, 501−518.

(48) Lousa, D.; Pinto, A. R. T.; Campos, S. R. R.; Baptista, A. M.; Veiga, A. S.; Castanho, M. A. R. B.; Soares, C. M. Effect of PH on the Influenza Fusion Peptide Properties Unveiled by Constant-PH Molecular Dynamics Simulations Combined with Experiment. *Sci. Rep.* **2020**, *10*, No. 20082.

(49) Lousa, D.; Soares, C. M. Molecular Mechanisms of the Influenza Fusion Peptide: Insights from Experimental and Simulation Studies. *FEBS Open Bio* **2021**, 3253−3261.

(50) Michalski, M.; Setny, P. Membrane-Bound Configuration and Lipid Perturbing Effects of Hemagglutinin Subunit 2 N-Terminus Investigated by Computer Simulations. *Front. Mol. Biosci.* **2022**, *9*, No. 826366.

(51) Humphrey, W.; Dalke, A.; Schulten, K. VMD: Visual Molecular Dynamics. *J. Mol. Graphics* **1996**, *14*, 33−38.

(52) Kabsch, W.; Sander, C. Dictionary of Protein Secondary Structure: Pattern Recognition of Hydrogen-Bonded and Geometrical Features. *Biopolymers* **1983**, *22*, 2577−2637.